Pergamon

Continental Shelf Research, Vol. 15, No. 1, pp. 59–88, 1995

0278–4343/95 $7.00+0.00

Buoyancy forced interaction between estuary and inner shelf: observation

KUO-CHUIN WONG* and ANDREAS MÜNCHOW*†

(*Received* 5 *January* 1993; *accepted* 24 *June* 1993)

Abstract—In May and June of 1990 we explored the hydrographic variability of the Delaware Estuary and the adjacent inner shelf with shipboard instruments. We found significant three-dimensional density variability both within the estuary and on the shelf. We found weak vertical stratification but strong transverse variability within the estuary, with denser water concentrating in the center of the estuary and two branches of lighter water near both shores. On the shelf, the buoyant estuarine water forms a southward flowing coastal current in the direction of Kelvin wave phase propagation (downstream). ADCP observations and thermal wind calculations indicate a flow of 10–20 cm s^{-1} downstream. Both the width of the coastal current and the magnitude of horizontal density gradients undergo substantial variations along the shelf.

1. INTRODUCTION

INCREASING evidence (GARVINE, 1991; PAPE and GARVINE, 1982) suggests that estuaries and the adjacent continental shelves are strongly coupled through the exchange of different water masses across the mouth of estuaries. The response to forcing in either the estuary or the shelf differs from systems where the two regimes are isolated from each other. The distribution of dissolved and particular matter within an estuary and the nearby ocean thus depends upon the circulation, the mixing and the dynamics of both regimes. We here report, analyze and interpret density and flow field observations from the Delaware Estuary and the nearby inner continental shelf of the Mid-Atlantic Bight. We extend the studies of GARVINE (1991), MÜNCHOW *et al.* (1992a, b), WONG and GARVINE (1984), and PAPE and GARVINE (1982) that all concentrate on the interaction of the Delaware Estuary with the nearby shelf. PAPE and GARVINE (1982) deployed surface and bottom drifters to demonstrate that the estuarine gravitational circulation (PRITCHARD, 1956; HANSEN and RATTRAY, 1965) extended well beyond the estuary onto the shelf. GARVINE (1991) quantified the near bottom shelf flow that agreed with barotropic model predictions of MASSE (1990). Near the surface, however, GARVINE (1991) reported mean flows in the direction opposite to those predicted by Masse's model. Instead, surface currents correlated well with freshwater discharge of the Delaware River, and GARVINE (1991) postulated a buoyancy driven coastal current on the shelf. MÜNCHOW and GARVINE (1993a,

*College of Marine Studies, University of Delaware, Newark, DE 19716, U.S.A.
†Present address: Center for Coastal Studies, Scripps Institution of Oceanography, University of California, La Jolla, CA 92093, U.S.A.

b) and MÜNCHOW (1992) described this current, its variability, and its dynamics. The measurements from all of these studies are confined to the inner shelf within 40 km from the mouth of the Delaware Estuary.

Our present study extends the above ones in four ways. First, we describe the density field of both the estuary and the shelf. Second, we examine the structure of the coastal current on the shelf more than 80 km from the mouth of the estuary. Third, we observe apparent instabilities of the coastal current for the first time; and fourth, we discover the presence of large lateral density gradients within the estuary.

Along with MÜNCHOW and GARVINE (1993a, b) and MÜNCHOW (1992), we find a buoyancy driven coastal current that contacts the bottom at all times. This observation distinguishes this coastal current from many others. Outflows from the Chesapeake Bay (BOICOURT, 1973; CHAO, 1990) and the Hudson–Raritan Estuary both detach from the bottom as do those along the coasts of Alaska (ROYER, 1983), Norway (JOHANNESON *et al.*, 1989), and Sweden (SHAFFER and DJURFELDLT, 1983). BLANTON (1981) and DE RUIJTER *et al.* (1991), however, report buoyancy driven coastal currents that appear similar to ours.

The salinity distribution within an estuary depends critically on the fresh water discharge and the characteristics of estuary–shelf interaction. The subject has attracted considerable research, such as those reviewed by FISCHER *et al.* (1979) and CHATWIN and ALLEN (1985). Most of these studies, however, focus on the longitudinal salinity distribution and assume lateral homogeneity. For the Delaware Estuary, GARVINE *et al.* (1992) report a longitudinal salinity distribution that depends only weakly upon the freshwater discharge into the estuary. Hence some powerful buffering agents must exist in order to reduce the salinity response. GARVINE *et al.* (1992) propose several possible mechanisms, with the action of lateral shear dispersion coupled to strong lateral salinity gradients (FISCHER, 1976; SMITH, 1980) being one of them. We here indeed observe large lateral salinity variations within the Delaware Estuary that could support the above mechanism.

We organize our study as follows. We introduce our study area and data sources in Section 2 and the observed variability in Section 3. In Section 3 we start with a description of the hydrography of the Delaware Estuary and the adjacent continental shelf. We then touch on details of the subtidal flow and density fields associated with the Delaware coastal current. We present velocity measurements from a shipboard acoustic doppler current profiler (ADCP). The novel screening and processing of the ADCP data, however, we defer to the appendix. Section 4 concludes this paper and compares its observational results with those from recent modeling studies.

2. THE STUDY AREA AND DATA SOURCES

The Delaware estuary (Fig. 1) is a major coastal plain estuary located on the east coast of the United States. It communicates with the Atlantic Ocean through a single 18 km wide mouth. The estuary is 215 km long, its upstream limit is the head of the tide at Trenton, New Jersey. The estuary reaches its widest point about 20 km upstream from the mouth, with a width of about 45 km. From that point the breadth of the estuary decreases nearly exponentially with distance upstream. The mean depth of the estuary is about 8 m. Multiple channels characterize the lower bay and fan out in a finger-like configuration. At

Fig. 1. Location map of Delaware Bay and the adjacent continental shelf. Bathymetry is in m.

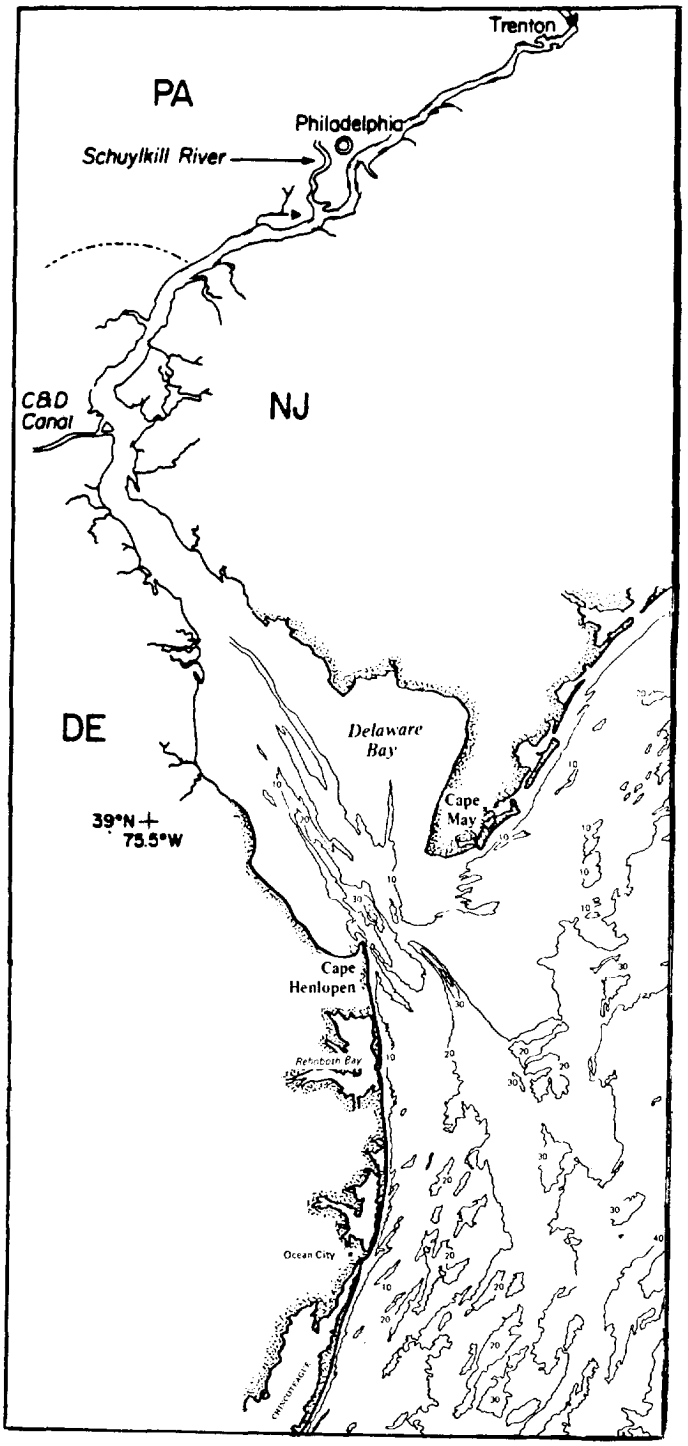
Trenton
PA
Philadelphia
Schuylkill River
C&D Canal
NJ
DE
Delaware Bay
Cape May
39°N +
75.5°W
Cape Henlopen
Rehoboth Bay
Ocean City

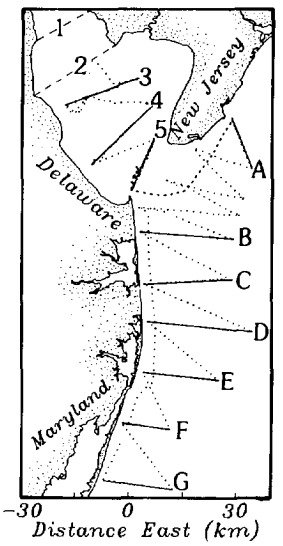

Fig. 2. The shiptrack of the R.V. *Cape Henlopen* during two cruises conducted on 22–24 May and 12–14 June 1990. The solid lines mark the CTD transects taken within the bay (transects 3–5) and on the inner shelf (transects A–G). CTD transects 1 and 2 were traversed with a small raft (see text).

the bay mouth the deep ancestral channel runs near Cape Henlopen and continues seaward to the southeast. The inner continental shelf off Delaware bay, defined here as the part of the continental shelf with depth less than 30 m, also exhibits complex bathymetry, with the ancestral Delaware River channel being a distinctive feature.

The Delaware River, gauged at Trenton, New Jersey, contributes approximately 60% of the total fresh water discharge into the estuary. The Schuylkill River, entering through Philadelphia, Pennsylvania, contributes another 15%. No other single source contributes more than 1% of the total fresh water discharge into the systems. Most of the fresh water thus enters the system in the upper reaches of the estuary. The discharge pattern in the Delaware River is seasonal. The average discharge at Trenton during spring and early summer is about 500 $m^3 s^{-1}$. The tidal motion is semi-diurnal and the M_2 tide enters the bay mouth with a tidal height amplitude of about 0.7 m. The amplitude of tidal volume flux is about $1.47 \times 10^5 m^3 s^{-1}$ (MÜNCHOW *et al.*, 1992a). The large ratio between the tidal and fresh water volume flux implies a weakly stratified estuary.

Our data sources originate from two cruises in 1990 which we conducted during 22–24 May, and during 12–14 June. Figure 2 shows the ship track of the R.V. *Cape Henlopen* along with annotated transects of the June cruise. The transects marked 1 and 2 were profiled from a small raft with a Seabird CTD, while all other transects were profiled with a Neil-Brown CTD. Typically there are between 8 and 10 vertical CTD profiles at each transect, resulting in transverse resolution of about 2 km. While the ship was underway, a thermosalinograph measured conductivity and temperature continuously from an intake 1 m below the surface. The cruise in May was more limited in scope, particularly in terms of CTD profiles taken on the inner shelf.

In May we also collected velocity data with a hull mounted ADCP. MÜNCHOW *et al.*

Table 1. *ADCP properties*

Acoustic frequency	307 kHz
Ping rate	1 Hz
Vertical bin size	4 m (2m)†
Pulse length	4 m (2m)†
Transducer depth	1 m
Blanking below transducer	3 m
Ship speed	5 m s^{-1}
Firmware version	16.32
DAS software version	2.48
Transducer misalignment α^*	−0.6°
Sensitivity constant β^*	1.0021

*Calibration Coefficients (JOYCE, 1989).
†Within the estuary.

(1992b) tested this instrument on the inner shelf. The set-up of the ADCP and its calibration coefficients we list in Table 1. Even though the ADCP provides vertical current profiles along the ship track, we here use the data to map horizontal current variability only. In Section 3 we thus present velocity data from a single bin only, namely that centered at 5 and 6 m below the surface inside the estuary and on the shelf, respectively. further details about the ADCP observations are provided in the appendix.

As suggested by the work of FUGLISTER (1955) regarding the temperature distribution of the Gulf Stream, different contouring algorithms may lead to significantly different contours for the same irregularly spaced data. We thus state our choices on interpolation details in Table 2. For the regularly spaced CTD data along transects we utilized the

Table 2. (*a*) *Interpolation: CTD transect data*

Interpolation method:	min. curvature
Grid size (depth, m):	1
Grid size (distance, km):	1
Weight of filter	r^{-1}
Weight at $r = 0$	1
Filter length	3 m × 3 km

(*b*) *Interpolation: the thermosalinograph data*

Interpolation method:	inverse distance
Weight	r^{-3}
Search radius:	30 km
Search angle:	45°
Number of data in sector:	10
Grid size (alongshore, km)	2.5
Grid size (across-shore, km)	1.25
Weight of filter	r^{-3}
Weight at $r = 0$	1
Filter length	5 km × 2.5 km

method of minimum curvature (BIGGS, 1974) which corresponds to a biharmonic spline interpolation technique (SANDWELL, 1987). This method, however, performs poorly for sparsely or very irregularly spaced data. Salinity along the shiptrack is irregularly spaced and we thus apply an interpolation technique which assigns weights to data corresponding to their inverse distance from a grid point. Since the coastal current is not homogeneous in space, we search for data in an ellipse with a ratio of minor to major axis or across- to along-shore distance of 1:2. This choice reflects prior knowledge of the coastal current. Finally, we spatially filtered all interpolated data to remove noise, but also to make our scale assumption as explicit as possible. Our surface salinity maps, for example, represent spatial variability only above 2.5 and 5 km in the across- and along-shore directions, respectively.

3. THE OBSERVED VARIABILITY

The hydrography of the Delaware Estuary

Most previous hydrographic observations in Delaware Bay were conducted along the major axis of the bay. GARVINE *et al.* (1992) examined long-term axial salinity records and revealed that the salinity decreases linearly between the bay mouth and a point roughly 90 km upstream. There the salt intrusion ends abruptly. The salinity distribution we observed along the deep channel of the estuary (not shown) is consistent with previous studies. The axial distribution reflects a weakly stratified estuary where fresh and warm riverine water from upstream interacts with cold and saline water from the shelf. The density distribution follows closely the salinity distribution. The relatively simple hydrography along the major axis of the Delaware Estuary, however, belies the complexity of the three-dimensional hydrographic distribution within the estuary that we describe next.

Our study represents the first systematic examination of the lateral hydrographic variability in the lower Delaware Bay. Figure 3 depicts five salinity sections across the bay, from transect 1 about 50 km upstream of the mouth to transect 5 at the bay mouth (see Fig. 2 for transect locations). The view is up-estuary, with the Delaware coast to the left. Most isohalines intersect the sea surface, indicating that lateral salinity variations dominate over vertical ones. In transect 2 we crossed a small scale front representing a lateral salinity gradient of more than 3 psu km^{-1}.

Even though the details of lateral structures differ from transect to transect, one dominant feature persists throughout all the transects: two branches of low salinity water hugging both shores are separated by high salinity water in the middle of the bay. At depth the saline waters dome up toward the surface to the right of the channel. The large lateral variability reflects the effect of estuary-shelf coupling within the lower bay, as fresher waters enter the estuary from upstream while saline waters enter from the shelf.

Figure 4 shows a T–S diagram which incorporates the CTD data from all lateral transects in the estuary. Here, we include data from both surveys. The data from May appear in the

Fig. 3. The distribution of salinity (in psu) across five lateral transects in lower Delaware Bay. Locations of the transects are shown in Fig. 2.

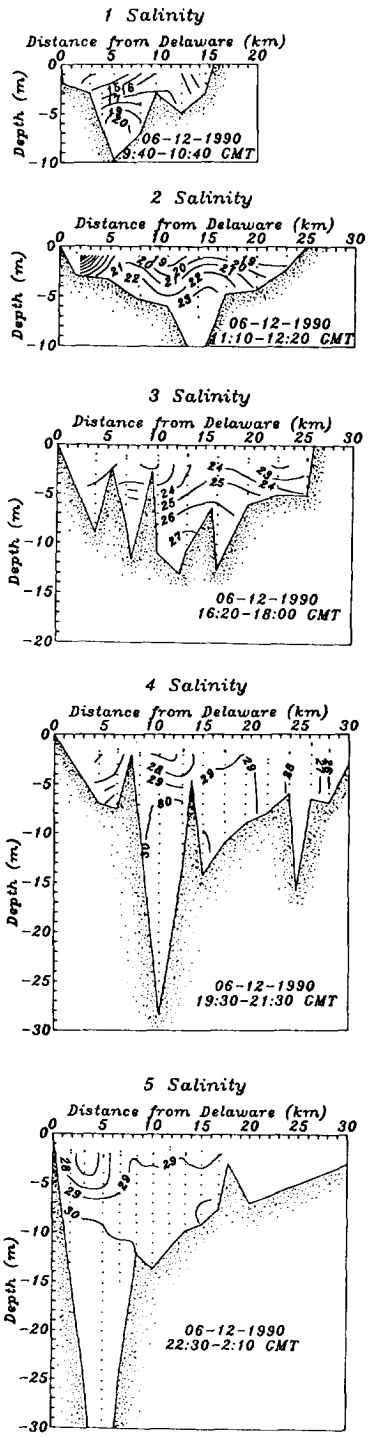
1 Salinity
Distance from Delaware (km)
0 5 10 15 20
Depth (m)
0 -5 -10
06-12-1990
9:40-10:40 GMT
2 Salinity
Distance from Delaware (km)
0 5 10 15 20 25 30
Depth (m)
0 -5 -10
06-12-1990
11:10-12:20 GMT
3 Salinity
Distance from Delaware (km)
0 5 10 15 20 25 30
Depth (m)
0 -5 -10 -15 -20
06-12-1990
16:20-18:00 GMT
4 Salinity
Distance from Delaware (km)
0 5 10 15 20 25 30
Depth (m)
0 -5 -10 -15 -20 -25 -30
06-12-1990
19:30-21:30 GMT
5 Salinity
Distance from Delaware (km)
0 5 10 15 20 25 30
Depth (m)
0 -5 -10 -15 -20 -25 -30
06-12-1990
22:30-2:10 GMT

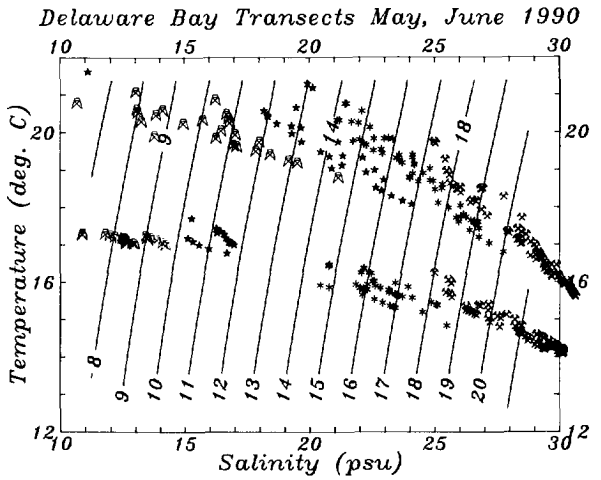

Fig. 4. *T–S* diagrams constructed from CTD profiles taken from transects 1–4 in lower Delaware Bay. Data from each transect are marked by a different symbol. The upper half of this figure shows the *T–S* relationship for the data collected in June, and the lower half of the figure shows the *T–S* relationship for the data collected in May.

lower half of the *T–S* diagram while those from June occupy the upper half. The *T–S* diagram exhibits a linear relationship between salinity and temperature for both months, with lower salinity corresponding to higher temperature, and vice versa. Figure 4 also exhibits the range of temperature and salinity variations of each transect. Much of this variation is due to the lateral, not the vertical structure. The offset between the data from May and those from June is caused by the seasonal warming between the 2 months. The *T–S* relationship in June also shows a larger slope relative to that in May. We reason that estuarine water upstream warms up faster than the shelf water further downstream as summer approaches.

Figure 5 shows a NOAA-11 AVHRR/MCSST image with a spatial resolution of 1.1 km. The image was taken on 12 June, concurrent with our field survey. The temperature structure within the lower bay shows intense lateral variability. At the widest part of the bay there is a 5°C across-bay temperature difference that along with Figure 4 we interpret as the intrusion of cool (and therefore saline) water up the bay and the presence of warm (and therefore fresh) water along both the Delaware and the New Jersey shores. This false color image provides a vivid visualization of the lateral variability in the entire lower bay.

We note that the observations of Fig. 3 were obtained during a period longer than 12 h. The salinity transects shown in Fig. 3 thus neither resolve tidal variability nor are they truly synoptic. These drawbacks are common problems of shipboard surveys in estuaries. Given the strong tidal motions in the Delaware Estuary with tidal excursions in excess of 10 km, it is important to examine whether the main features in Fig. 3 are strongly influenced by the tides or not. Over a 13 h period on 14 June 1990, we repeatedly profiled transect 5 where the tidal motion is strongest. We traversed the bay mouth 11 times and each time we took CTD profiles at 10 stations along the transect at roughly 1.8 km intervals. Given that the dominant tidal constituent is M_2 with a Nyquist frequency of about 4 cycles per day, we feel

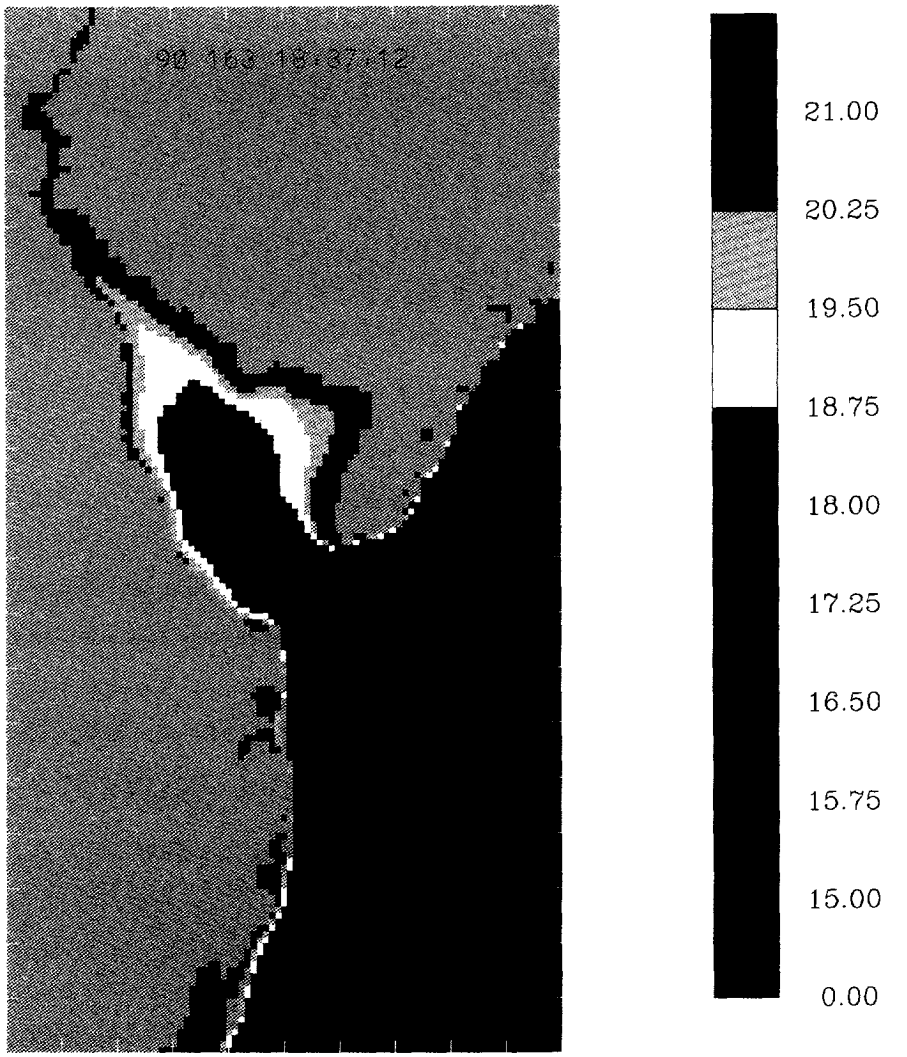

Fig. 5. False colour NOAA-11 SST image over Delaware Bay for 12 June 1990. Temperature scale (in °C) is on right. The warm temperatures along the Delaware and the New Jersey shores mark the two branches of low salinity water within the bay.

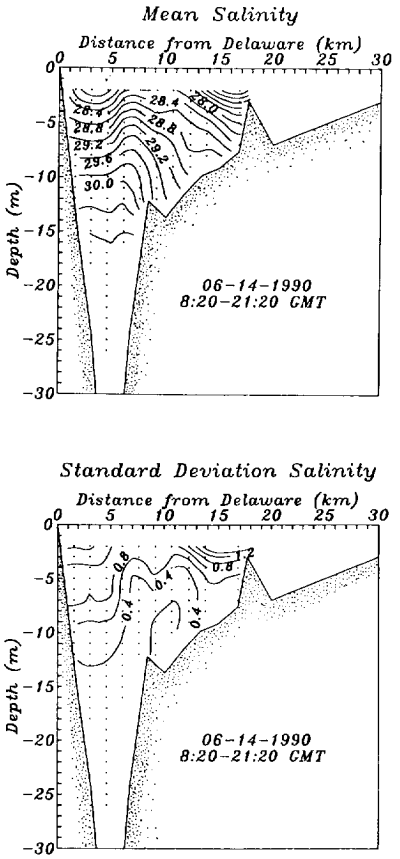

Fig. 6. The tidally averaged mean salinity distribution at the bay mouth (top panel) and the standard deviations around the mean (lower panel).

that such a sampling scheme provides sufficient temporal resolution for the hydrographic variation over a semidiurnal tidal cycle.

Figure 6 (top panel) shows the tidally averaged salinity distribution across the bay mouth. We find high salinity water over the deep channel that domes up toward the surface to the right of the channel. This high salinity water separates two branches of low salinity water along the Delaware and New Jersey shores. The tidally averaged features, including the horizontal split in the hydrographic distribution, correspond closely to those in Fig. 3. We note, however, that the standard deviations (Fig. 6, lower panel) from the tidally averaged distribution indicate the presence of large intratidal variability.

As salinity is an excellent tracer of estuarine water, we next use its distribution to infer the structure of the residual circulation. At the mouth of the Delaware estuary, Fig. 6 implies the presence of two branches of low salinity estuarine outflows along the shores that are separated by the inflow of high salinity shelf water over the deep channel. This flow pattern contradicts the conventional idea of a two-layer estuarine gravitational circulation with a low salinity surface outflow and a high salinity bottom inflow. A number of mechanisms can produce lateral structure in the residual circulation. The internal

Rossby radius (L_D) of the Delaware estuary is about 5 km. The width of the lower estuary (W) is significantly larger than L_D. With a ratio of $W/L_D > 1$, we expect the Coriolis force to partly deflect the light, low salinity water against the Delaware shore. The Coriolis effect, however, cannot explain the estuarine outflow along the New Jersey shore. We will now show that lateral variations in bottom bathymetry may be crucial in establishing the observed lateral structure.

PRITCHARD (1956) was the first to propose the simplest longitudinal momentum balance for the gravitational circulation as

$$0 = -\frac{1}{\rho_o}\frac{\partial p}{\partial x} + A_z\frac{\partial^2 u}{\partial z^2}. \tag{1}$$

Equation (1) represents a balance between the tidally averaged horizontal pressure gradient and the vertical shear stress associated with the gravitational circulation. Here ρ_o is an averaged density, p is the pressure, A_z is a constant vertical eddy viscosity, and u is the longitudinal (x) component of the gravitational circulation. We adopt a left-handed coordinate system at the mouth of the estuary. The origin of the coordinate system is located at the surface in the middle of the cross section. Here x is positive out of the estuary, y is positive to the right as one looks up-estuary, and z is positive down toward the bottom.

By taking the derivative of equation (1) with respect to z and noting that the horizontal pressure gradient consists of a baroclinic and a barotropic component, we obtain

$$0 = -\frac{g}{\rho_o}\frac{\partial \rho}{\partial x} + A_z\frac{\partial^3 u}{\partial z^3}. \tag{2}$$

If the horizontal density gradient $\partial\rho/\partial x$ is known, the distribution of u across the mouth of the estuary can be solved with the following boundary conditions:

$$\frac{\partial u}{\partial z} = 0 \quad \text{at} \quad z = 0 \tag{3}$$

$$u = 0 \quad \text{at} \quad z = H \tag{4}$$

$$\int_{-B}^{B}\int_{o}^{H} u \, dz \, dy = 0. \tag{5}$$

Equation (3) indicates the no-stress condition at the surface ($z = 0$), equation (4) represents the no-slip condition at the bottom ($z = H$), and equation (5) expresses the continuity equation with the assumption that the river discharge is much smaller than the volume flux of the gravitational circulation. We have neglected many processes which also contribute to the residual circulation. We here examine the effect of density-driven gravitational circulation due to an axial pressure gradient and bottom friction only.

A rather conventional assumption about gravitational circulation is that one can ignore the lateral variation in u. In our application, lateral homogeneity can only be satisfied if the estuary has a rectangular cross-section (H = constant). With such an assumption, equation (5) can be simplified as $\int_o^H u \, dz = 0$, and the solution for u has been solved by OFFICER (1976) as

$$u(z) = \frac{g}{\rho_o A_z}\frac{\partial \rho}{\partial x}\frac{H^3}{48}\left[8\left(\frac{z}{H}\right)^3 - 9\left(\frac{z}{H}\right)^2 + 1\right]. \tag{6}$$

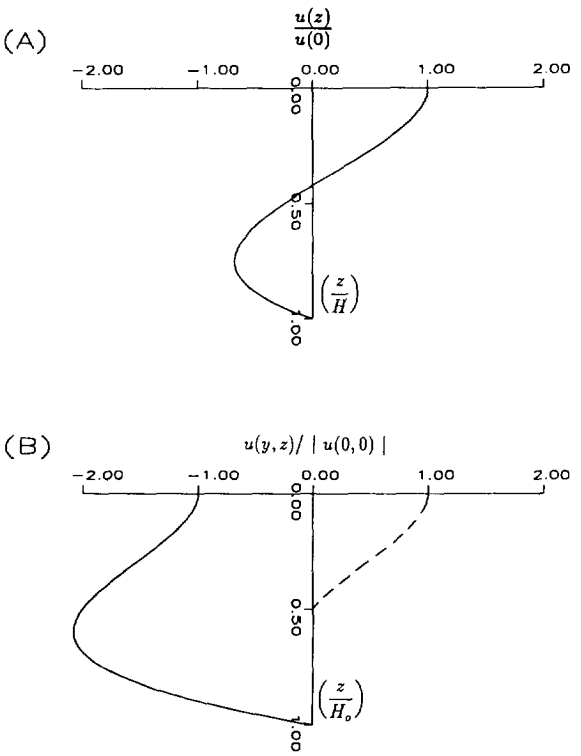

Fig. 7. (A) The distribution of normalized residual current $u(z)/u(0)$ in an estuary with a rectangular cross-section. The current is assumed to be laterally homogenous; positive values indicate seaward motion. (B) The distribution of normalized residual current $u(y,z)/|u(0,0)|$ at two points across an estuary with a triangular cross-section. The solid curve to the left indicates the vertical distribution of current at the center of the cross section ($y = 0$). The dashed curve to the right indicates the current distribution at $y = 0.5B$ (see text).

At the surface the current is

$$u(o) = \frac{g}{\rho_o A_z} \frac{\partial \rho}{\partial x} \frac{H^3}{48}.$$

Since $\partial\rho/\partial x$ is positive (salinity increases downstream), the surface current is positive and flows out of the estuary. Figure 7(A) shows the distribution of $u(z)/u(o)$ vs normalized depth (z/H). A two-layer circulation emerges, with the surface and bottom layers flowing out of and into the estuary, respectively.

The flow field of equation (6) is consistent with the conventional two-layer gravitational circulation as described by PRITCHARD (1956) and HANSEN and RATTRAY (1965). The two-layer flow structure depends critically on the assumption of a rectangular cross-section. A rectangular cross-section, however, is often a very poor approximation for many major estuaries. This is especially true for estuaries formed by drowned river valleys, such as the Delaware estuary, where the cross-sections are often triangular, with a deep channel in the center and shallow depth along the shores (DYER, 1973; see also Fig. 6). We next explore

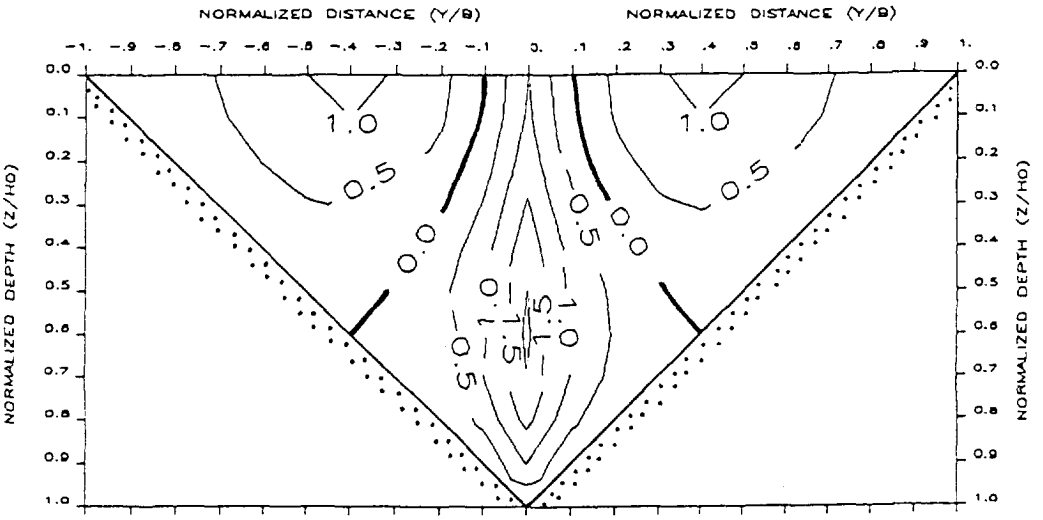

Fig. 8. The distribution of normalized gravitational circulation $u(y,z)/|u(0,0)|$ in an estuary with a triangular cross-section. Positive values indicate seaward outflow and negative values indicate landward inflow. The highlighted contour lines of zero velocity mark the separation between inflow and outflow.

the effect of such across-estuary bathymetry on the structure of gravitational circulation and offer an explanation for the observed split of buoyant waters in the Delaware Estuary.

Consider an estuary with a triangular cross-section, where the depth decreases linearly from $H = H_o$ at the center of the cross-section ($y = 0$) to $H = 0$ at the shores ($y = \pm B$). Based on equations (2), (3), (4) and (5), the current normal to the cross-section can be expressed as

$$u(y, z) = \frac{g}{\rho_o A_z}\frac{\partial \rho}{\partial x}\frac{H_o^3}{60}\left\{10\left[\left(\frac{z}{H_o}\right)^3 - \left(1 - \frac{y}{B}\right)^3\right] - 9\left[\left(\frac{z}{H_o}\right)^2 - \left(1 - \frac{y}{B}\right)^2\right]\right\}. \tag{7}$$

Equation (7) is valid for the region $y = 0$ to $y = B$ where $H(y) = H_o(1 - (y/B))$. The solution for $y = 0$ to $y = -B$ is a mirror image of equation (7). The current as described by equation (7) varies laterally, as u is now a function of both y and z. In addition, the vertical structure of u scales with the maximum depth of the cross-section H_o, not the mean depth of the estuary. At the center of the cross-section ($y = 0$), the flow at the surface ($z = 0$) is now

$$u(0, 0) = -\frac{g}{\rho_o A_z}\frac{\partial \rho}{\partial x}\frac{H_o^3}{60}. \tag{8}$$

Since $\partial\rho/\partial x > 0$, $u(0, 0) < 0$. This indicates that at the center of the estuary even the surface current is directed up the estuary.

The solid curve in Fig. 7(B) shows the distribution of $u(y, z)/|u(0, 0)|$ at $y = 0$. The flow is directed into the estuary throughout the water column except at the bottom where the current vanishes. The dashed curve in Fig. 7(B) shows the distribution of $u(y, z)/|(u(0, 0)|$ at $y = 0.5B$, and the current structure shows unidirectional flow out of the estuary at all depths.

Figure 8 shows the overall structure of $u(y, z)/|u(0, 0)|$ throughout the entire cross-section of the estuary. Instead of a two-layer circulation, the gravitational circulation is now dominated by a lateral structure with inflow (negative values) concentrating in the deep channel and outflows (positive values) in the shallow areas along the shores. Note that a flow reversal with depth, with a surface outflow and a bottom inflow, occurs only in a very limited region along the cross section.

Shelf water that enters an estuary is often more salty than the brackish water that exits the estuary. Hence Fig. 8 implies two branches of low salinity water that flow along the shores are separated by saline water in the middle of the estuary over the deep channel. This distribution is at least qualitatively consistent with the observed hydrography across the mouth of Delaware Bay.

The hydrography of the inner shelf

The buoyant water that exits the estuary imposes a strong forcing onto the inner continental shelf. In particular, the branch of the low salinity water along the Delaware shore constitutes the source water for the coastal current reported by MÜNCHOW and GARVINE (1993a, b) and GARVINE (1991). While previous studies tackled the coastal current some 40 km downstream from the estuary, we here report evidence of buoyant water more than 80 km downstream.

In Fig. 9 we present the salinity distribution at the bay mouth (transect 5) as well as that across the inner shelf transects A–G (see Fig. 2 for locations). MÜNCHOW *et al.* (1992b) reported that subtidal currents at the mouth of the estuary transport buoyant waters seaward in a narrow region off Delaware with speeds up to 20 cm s^{-1}. The salinity distribution at transect 5 clearly indicates that buoyant water occupies a narrow and shallow pool near the Delaware coast. This is the estuarine outflow that we will trace more than 80 km downstream. At transect 5 the buoyant water is detached from the bottom due to the deep channel there.

After exiting the bay mouth, the outflow deepens, comes in full contact with the bottom, turns anti-cyclonically and forms the coastal current (Fig. 9, transects B and C). Thereafter, the width of the coastal current undergoes substantial variation with distance along the shelf. Starting from a width of 5 km at the bay mouth, the coastal current widens to 25 km at a distance of 40 km downstream (transect D). Then it narrows to 12 km at transect F only to grow again to about 20 km in width at transect G. The across-shelf salinity gradient changes with the width of the coastal current. Over the first 40 km the across-shelf salinity gradient decreases as the coastal current widens. Further downstream the salinity gradient increases as the width of the coastal current contracts. At transect F the coastal current reaches its narrowest point on the shelf, and all the seaward sloping isohalines coalesce and form a well-defined frontal boundary separating the buoyant estuarine outflow from the ambient shelf water.

In Fig. 10 we present the T–S diagrams for all the CTD profiles shown in Fig. 9. At the bay mouth (transect 5) the temperature and salinity exhibit a strong linear relationship, with lower salinity corresponding to higher temperature, and vice versa. At the inner shelf transect nearest to the bay mouth (transect B), the T–S diagram indicates the presence of coastal current and ambient shelf water. The coastal current is represented by the data points with salinity lower than 31 psu, and the T–S relationship for these points resembles those at the bay mouth. For data points with salinity higher than 31 psu, the T–S line slopes

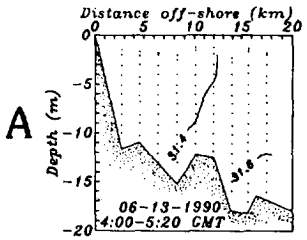
A
Distance off-shore (km)
Depth (m)
06-13-1990
4:00-5:20 GMT

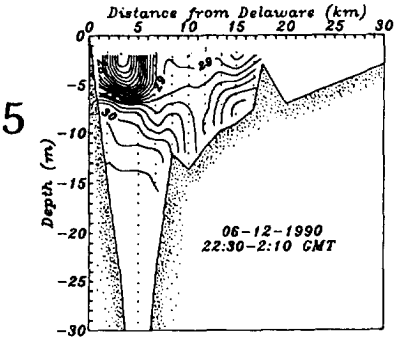
5
Distance from Delaware (km)
Depth (m)
06-12-1990
22:30-2:10 GMT

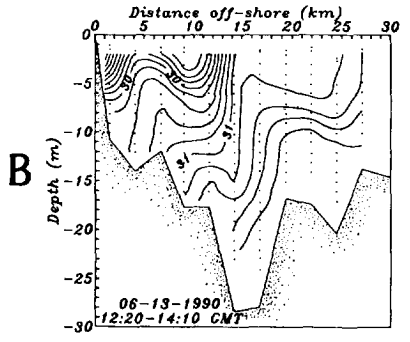
B
Distance off-shore (km)
Depth (m)
06-13-1990
12:20-14:10 GMT

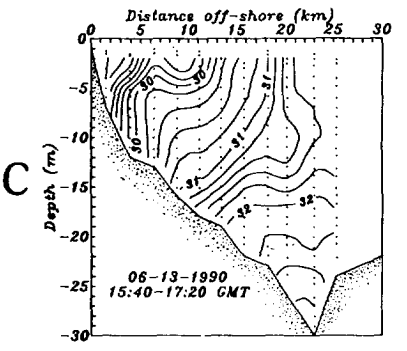
C
Distance off-shore (km)
Depth (m)
06-13-1990
15:40-17:20 GMT

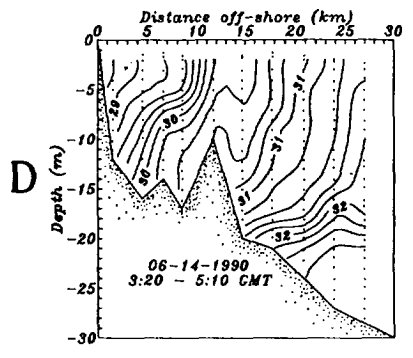
D
Distance off-shore (km)
Depth (m)
06-14-1990
3:20 - 5:10 GMT

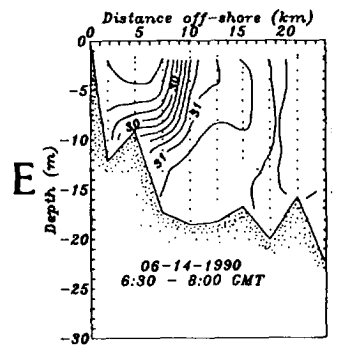
E
Distance off-shore (km)
Depth (m)
06-14-1990
6:30 - 8:00 GMT

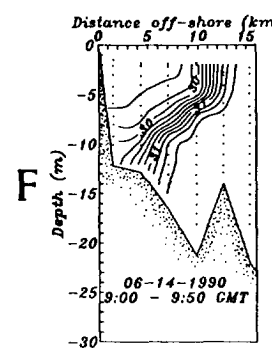
F
Distance off-shore (km)
Depth (m)
06-14-1990
9:00 - 9:50 GMT

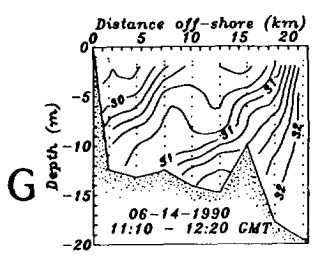
G
Distance off-shore (km)
Depth (m)
06-14-1990
11:10 - 12:20 GMT

differently, with large variations in temperature but little variations in salinity. These data represent the ambient shelf water. The large temperature variation is caused by the establishment of the seasonal thermocline in June. We thus conclude that on the inner shelf south of the estuary the *T–S* diagrams indicate three distinct water types. Closest to the estuary (transect B) the coastal current water is a mixture of estuarine and mixed shelf water, while the ambient shelf water is a mixture of surface shelf and bottom shelf water. Note that at transect B warm surface shelf water and warm estuarine water do not mix. Surface shelf water thus does not enter the estuary. On the shelf we thus find three water types, the surface shelf water, the bottom shelf water, and the brackish estuarine water.

The *T–S* diagram provides evidence for the clear separation of the coastal current water from the ambient shelf water. This basic pattern of *T–S* distribution persists from transect B to transect D downshelf. The data are somewhat scattered since mixing takes place as the coastal current expands in width. At transect E the *T–S* relationship shows little scattering since the horizontal gradients increase and the coastal current contracts. Along transects F and G we do not resolve the ambient shelf waters well due to the limited seaward extent of our transects. There the *T–S* diagrams reflect the coastal current only.

The coastal current

We now present surface salinity and temperature distributions for the entire study area and flow field estimates from the ADCP. Most of the significant features of estuary-shelf coupling are reflected in the surface salinity distribution (Fig. 11). This is not surprising, as the horizontal variability is strong while vertical stratification is relatively weak. Within Delaware Bay salinity varies linearly with temperature. Cold, salty water intrudes the estuary near the center of the bay while warm, fresh waters flow along the Delaware and New Jersey shores. On the shelf, however, the linear relationship between surface salinity and temperature breaks down due to uniform thermal heating which masks surface temperature features. Nevertheless, the band of low salinity water exiting the estuary along the Delaware shore and forming the coastal current is the prominent feature of our study area.

All the above results originate from our survey in June, but represent those from an experiment 3 weeks earlier as well. In May we also collected velocity data with a hull mounted 307 kHz ADCP while the ship steamed with speeds up to 12 knots. We use only data from profiles where the ADCP tracked the bottom as we sailed in the direction of the swell. Nevertheless, we collected enough reliable velocity profiles to remove tidal currents from the data, as we surveyed the shelf twice while moving downshelf and back. In Fig. 12 we present subtidal current estimates from the ADCP at positions where the data passed all our screening criteria (Table 3). We fit the tidal currents to biharmonic splines at seven locations (knots) where they represent a least-square fit to the data (CANDELA *et al.*, 1990, 1992; FOREMAN and FREELAND, 1991; SANDWELL, 1987). Smooth behavior between these knot positions is guaranteed and is not a result. Our fit explains 87% of the current variance. MÜNCHOW *et al.* (1992b) estimated that errors in the subtidal current estimation are about 10% of the tidal signal (single ADCP measurement). Tidal currents exceed 100 cm s^{-1} in the estuary, and we thus expect uncertainties there as large as the subtidal

Fig. 9. Distribution of salinity (in psu) across transect 5 at the bay mouth and transects A–G on the inner shelf.

A

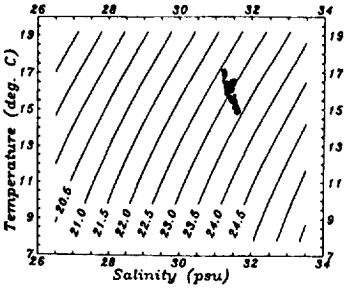
Temperature (deg. C)
Salinity (psu)

5

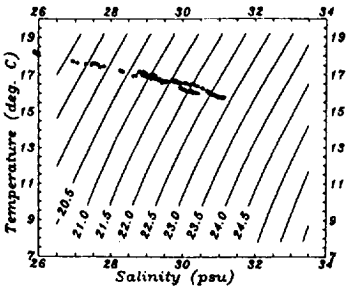
Temperature (deg. C)
Salinity (psu)

B

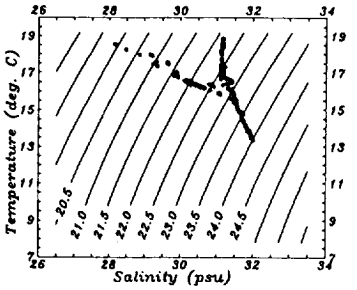
Temperature (deg. C)
Salinity (psu)

C

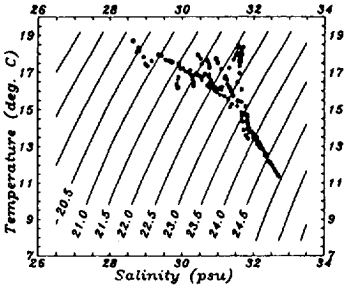
Temperature (deg. C)
Salinity (psu)

D

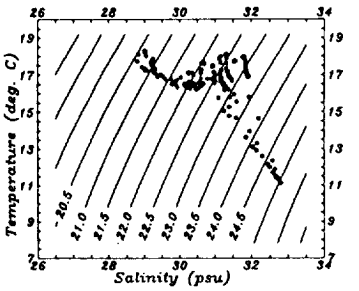
Temperature (deg. C)
Salinity (psu)

E

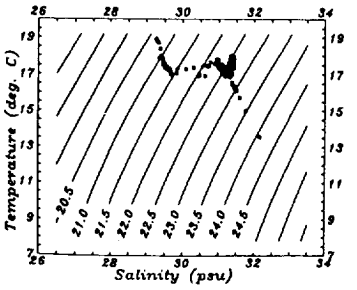
Temperature (deg. C)
Salinity (psu)

F

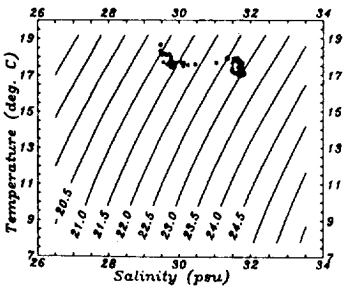
Temperature (deg. C)
Salinity (psu)

G

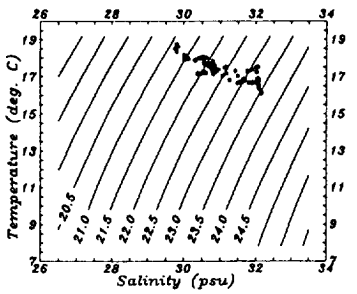
Temperature (deg. C)
Salinity (psu)

Table 3. ADCP data screening

Good pings	>85%
Change in ship heading	<2.0 degree min^{-1}
Change in ship speed	<1.5 knots min^{-1}
Ship speed	>2.0 knots

currents themselves, about 10 cm s^{-1}. On the shelf, however, tidal currents rarely exceed 20 cm s^{-1}. We thus expect subtidal currents to be accurate within 2–3 cm s^{-1}. Following CANDELA *et al.* (1992), we have also pursued a different error estimation technique, and the results are presented in the appendix along with more details of the ADCP data and its processing. In summary, we feel that the currents shown in Fig. 12 reliably represent the subtidal flow field on the inner shelf. They agree well with previously published current estimations (PAPE and GARVINE, 1982; GARVINE, 1991; Münchow *et al.*, 1992b).

In Fig. 12 we overlay the subtidal velocity estimates with a map of surface salinity. The hydrographic data were collected simultaneously with the ADCP velocity data. Note that the coastal current again widens on the shelf before it suddenly narrows 40 km downstream. This appears to be a robust feature of the coastal current. The flow field indicates the presence of the coastal current on the shelf as we observe a 5–10 km wide jet flowing downstream with speeds up to 20 cm s^{-1}. The flow closely follows salinity isolines and confirms the narrowing of the coastal current to be an advective phenomenon due to an onshore flow.

MÜNCHOW and GARVINE (1993b) analyzed dynamical properties of this coastal current and separated a source from a plume region. As we introduce a third region, where the plume narrows and forms a coastal jet, we first review the former two. From repeatedly profiled transects over several tidal cycles in April, 1989, MÜNCHOW and GARVINE (1993b) obtained subtidal estimates of the velocity and the density field. From these data they identified a frontal source region near the mouth of the estuary where the non-linear advection of seaward momentum appears important. Downstream on the shelf where the buoyant water widens, they find an almost linear flow in geostrophic balance across the shelf. In Fig. 13 we reproduce results from this downstream transect. The location of this transect is the same as D in Fig. 2. We show the subtidal density distribution, the calculated thermal wind current (u_g), and the measured along-shelf component of the subtidal current (u_m).

In the thermal wind calculations

$$u_g(y, z) = u_m(y, z_o(y)) + \int_{z_o}^{z} \frac{g}{\rho f}\left(\frac{\partial \rho}{\partial y}\right) dz. \tag{9}$$

MÜNCHOW and GARVINE (1993b) used the measured velocity u_m closest to the bottom as a reference for the geostrophic current that is calculated from the across-shelf density gradient $\partial\rho/\partial y$. The so computed geostrophic along-shelf currents [Fig. 13(b)] match the observed ones [Fig. 13(c)] well. The good correspondence, however, crucially depends on

Fig. 10. *T–S* diagrams constructed from the CTD profiles taken from transect 5 at the bay mouth and transects A–G on the inner shelf. Transect A is to the north of Delaware Bay.

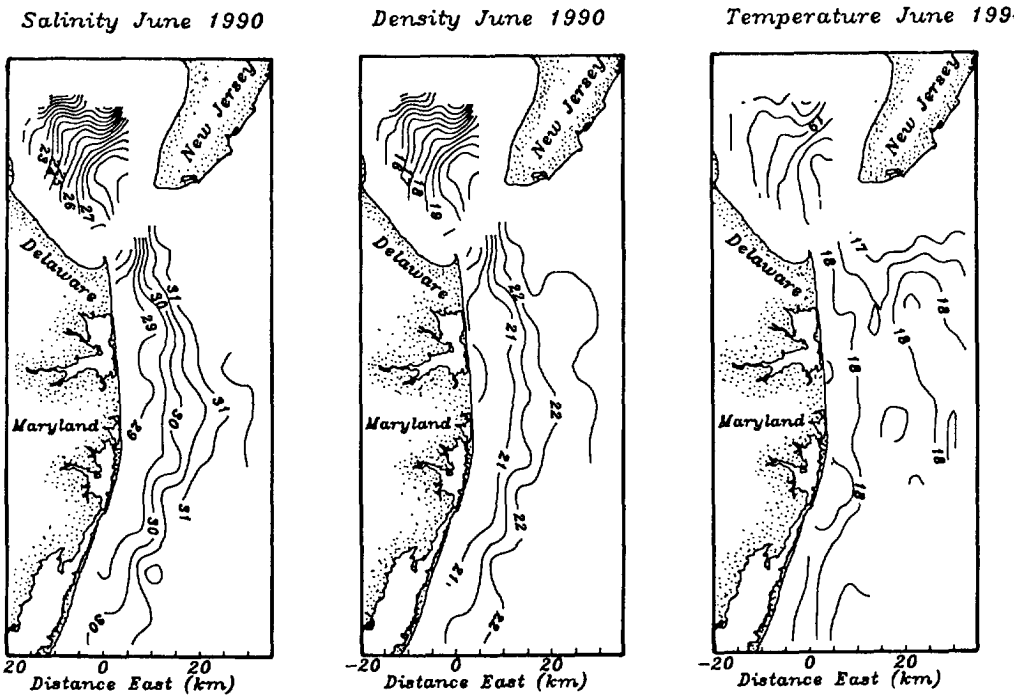

Fig. 11. Surface distributions of salinity (psu), density (σ_t), and temperature (°C) in lower Delaware Bay and the adjacent continental shelf.

the absence of wind generated motion (MÜNCHOW and GARVINE, 1993a; MÜNCHOW, 1992). Both in April 1989 and in June 1990 winds were weak (<1 m s^{-1}) and we feel confident that along-shelf currents in June 1990 can be computed from density transects based on across-shelf geostrophy. Figure 14 depicts both the density transects and the geostrophic velocities relative to no flow at the bottom. The along-shelf geostrophic currents exceed 15 cm s^{-1} and are consistent with the ADCP data (Fig. 12) that we collected 3 weeks prior. The along-shelf variability of the current, however, is dramatic. At transect D [Fig. 14(a)] we observe two distinct jets that a topographic feature apparently separates. Downstream at transects E and F the coastal current narrows, intensifies, and is next to the coast. We identify this as the coastal jet region that we alluded to above. The coastal jet, however, appears to be unstable as it meanders, and transect G shows a weaker, but wider current that resembles the flow at transect D. Note also the $\sigma_t = 22.0$ kg m^{-3} contour intersects the surface at 15, 11, 10 and 18 km from the coast at transects D–G, respectively. Given a tidal excursion of less than 2 km in the region, this meander is apparently caused by factors other than the tidal distortion.

From the data shown in Fig. 14 we next estimate dynamical parameters that characterize the flow in the coastal jet region. From the vertical density profiles we compute the stability frequency $N = \sqrt{-g[(\partial\rho/\partial z)/\rho_o]}$, from which we estimate the internal deformation radius $L_D = N \cdot D/f$, where D and f are the local water depth and Coriolis parameter, respectively. The ratio of L_D to L (the width of the current) then defines a Burger number $S = (L_D/L)^2$. This parameter is frequently used to describe stability properties of

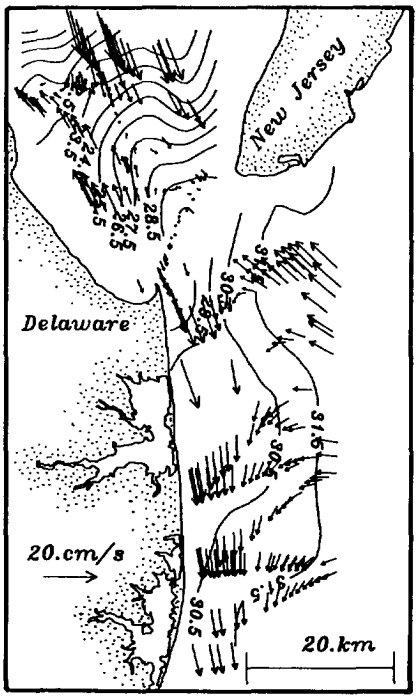

Fig. 12. Subtidal current vectors estimated from the ADCP observations in the study area (see text). The contour lines (in psu) indicate the surface salinity distribution. Both the ADCP and hydrographic data were collected in May 1990.

buoyancy driven coastal currents (GRIFFITHS and LINDEN, 1981; CHABERT D'HIERES *et al.*, 1991; MÜNCHOW and GARVINE, 1993b). We find Burger numbers that are always less than 0.25. The flow is then only weakly stratified. Another important parameter, the Rossby number $\varepsilon = U/Lf$, we estimate by using the sectionally averaged geostrophic velocity as U. We find the Rossby number to vary between 0.03 and 0.09, i.e. non-linear inertial forces appear to be unimportant. In summary, we list all scales and parameters in Table 4 and find that $\varepsilon \sim S \ll 1$. For such conditions HOGG (1973) showed that vortex tube stretching generates depth independent relative vorticity. The bottom topography then affects the

Table 4. Scales and parameters for the coastal jet region

Transect	D	E	F	G
L_D (km)	6.3	4.1	5.1	5.3
L_i (km)*	0.8	1.0	0.4	0.9
L (km)	15	11	10	18
U (cm s^{-1})	3.8	7.0	2.7	7.2
S	0.16	0.13	0.25	0.08
ε	0.03	0.09	0.03	0.06

*Inertial radius u/f.

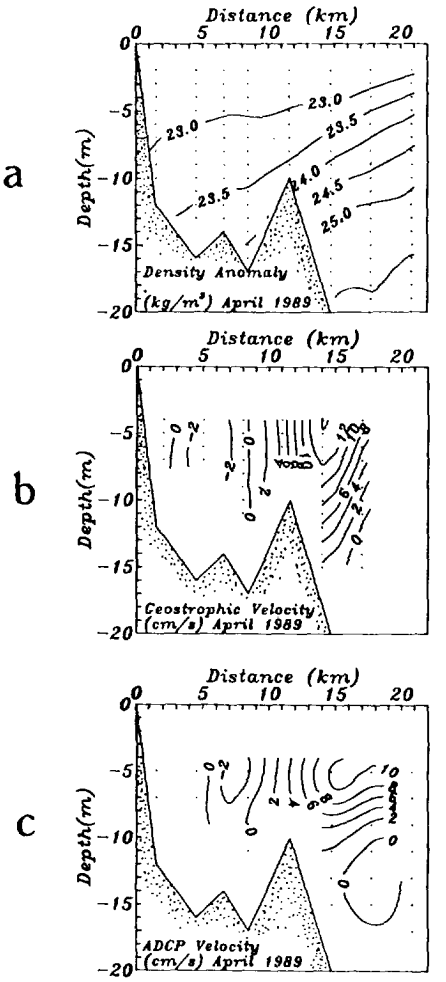

Fig. 13. Thermal wind diagnostics for data collected along transect D in April, 1989 (MÜNCHOW and GARVINE, 1993b). (a) Density anomaly, (b) thermal wind speeds normal to the transect, and (c) ADCP speeds normal to the transect.

entire water column and the flow tends to turn anti-cyclonically around shallow topography. This may explain the stronger off-shore jet at transect D or G, but not at F. The dynamics of the observed meanders and possible instabilities then need further, more theoretical, studies. These are beyond the scope of this paper. As a first step we suggest to employ the formalism of CUSHMAN-ROISIN (1986) as it allows a geostrophic flow with finite layer perturbations that we observe. In contrast, quasi-geostrophic theory (GRIFFITHS and LINDEN, 1981) is not applicable here as it requires small perturbations of both bottom topography and layer thickness (FLIERL, 1984).

4. CONCLUSIONS

The influx of freshwater into the Delaware Estuary constitutes an important forcing mechanism for the estuary and the shelf beyond. We have reported on the spatial

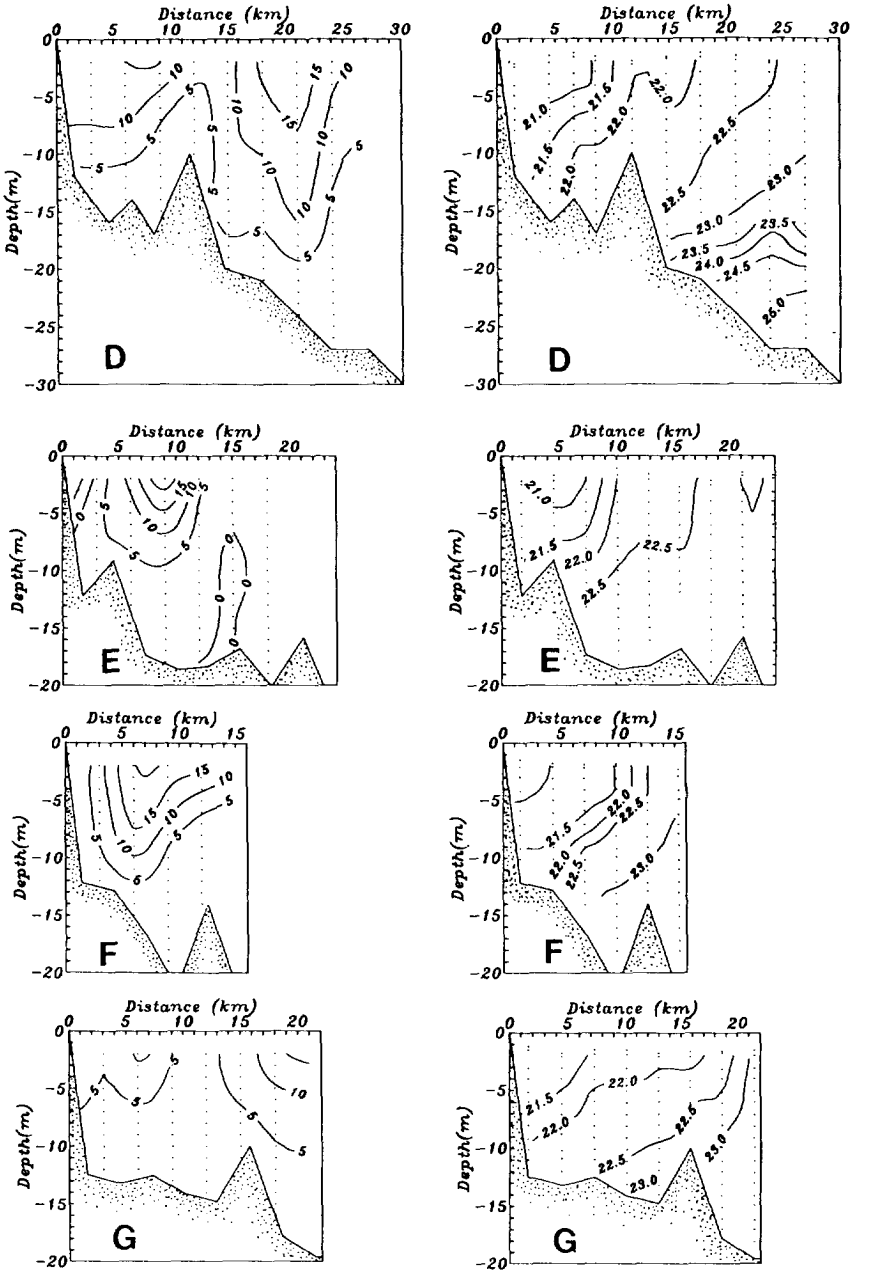

Fig. 14. Thermal wind diagnostics for data collected along transects D–G in June 1990. The left panel shows the thermal wind speeds normal to the transects, and the right panel shows the corresponding density anomalies.

distribution of properties and their scale of variability. Our observations emphasize lateral variability both within the wide estuary and on the shelf. This variability scales well with the internal deformation radius that is of the order of 5 km. In the estuary we find fresher and lighter water near both coasts while saline, heavier water occupies the central channel. The spatial coverage of our field observations was not sufficient to resolve the effect of the New Jersey branch of the low salinity estuarine water on the inner shelf hydrography. The buoyant water along the Delaware shore exits the estuary, turns anti-cyclonically, and subsequently forms a coastal current on the shelf that flows in the direction of Kelvin wave phase propagation. The current approaches speeds of 20 cm s^{-1}, extends 80 km along the shelf, and becomes unstable about 40 km from the mouth of the estuary. Thermal wind dynamics diagnose the along-shelf current well. Both Rossby and Burger numbers are small, i.e. the flow is almost linear and only weakly stratified.

GALPERIN and MELLOR (1990) recently conducted a modeling study in an attempt to realistically simulate the flow and density fields of the Delaware Estuary and the adjacent shelf for 1984. As both the freshwater discharge rates and the local wind stresses in May and June 1984 compare well with those in 1990, we next compare our observations with their model predictions.

The model is fully three-dimensional and includes an advanced turbulence closure scheme (MELLOR and YAMADA, 1982). It prescribes boundary conditions from data, uses real bottom topography, and resolves scales of 1 and 4 km within the estuary and on the shelf, respectively. A matching condition is placed at the mouth of the estuary.

Within the estuary the model predicts saline water near the coast of Delaware and fresher water near that of New Jersey for both up- and down-welling favorable winds blowing over the shelf (GALPERIN and MELLOR, 1990, p. 273). In contrast, we here report fresher water on both sides of the estuary. GALPERIN and MELLOR (1990) then predict currents that advect buoyant material in the direction of the prevailing winds (i.e. in the direction opposite to that of Kelvin wave phase propagation). In contrast, for the inner shelf south of the bay mouth, we observe buoyant material that is advected only in the direction of Kelvin wave propagation. Furthermore, MÜNCHOW and GARVINE (1993b) find a 3 month mean flow of about 10 cm s^{-1} on the shelf that opposes the mean winds. It thus appears that the model may have underestimated the strength of the buoyancy forced circulation. We suspect that both the matching condition and the spatial grid scale on the shelf (4 km) may have contributed to the discrepancies. The mouth of the estuary, where GALPERIN and MELLOR (1990) apply their matching condition, is the region where properties of the flow and the dynamics change most rapidly. On the shelf the spatial grid spacing of 4 km barely resolves the internal deformation radius. Our observation may then guide future modeling studies that adequately represent buoyancy forcing in a coupled estuary–shelf system. The horizontal split of the lateral density distribution inside the estuary, its sudden termination near the mouth, the formation of a coastal current, and the evolving instabilities of the latter all warrant further observational and theoretical studies. The interaction of estuary and shelf as a coupled system thus remains a challenge for coastal oceanographers.

Acknowledgements—We thank Richard W. Garvine for many helpful discussions through the course of this study. Joy Moses-Hall and Leslie Bender III provided valuable assistance regarding data collection and the subsequent data processing. Timothy Pfeiffer provided excellent technical assistance aboard the ship. The

dedication of Captain Donald McCann and the crew of the R.V. *Cape Henlopen* is appreciated. Claudia Ferdelman developed the software for some of the data analysis and graphics. Sheila Rollings typed the manuscript. K.-C. Wong and A. Münchow acknowledge the support by the National Science Foundation under Grant OCE-9000158 and OCE-8816009, respectively. Partial support was also provided by the NOAA Sea Grant under grant NA 16RG0162-02 (Project R/F-3) and the College of Marine Studies, University of Delaware, Newark, Delaware.

REFERENCES

BENDAT J. S. and A. G. PIERSOL (1980) *Engineering applications of correlation and spectral analysis*, Wiley, New York, NY, 302 pp.

BIGGS J. C. (1974) Machine contouring using minimum curvature. *Geophysics*, **39**, 39–48.

BLANTON J. O. (1981) Ocean currents along a nearshore frontal zone on the continental shelf of the eastern United States. *Journal of Physical Oceanography*, **11**, 1627–1637.

BOICOURT W. C. (1973) The circulation of water on the continental shelf from Chesapeake Bay to Cape Hatteras, Ph.D. thesis, Johns Hopkins University, Baltimore, MD, 183 pp.

CANDELA J., R. C. BEARDSLEY and R. LIMEBURNER (1990) Removing tides from ship-mounted ADCP data, with application to the Yellow Sea. In: *Proceedings of the IEEE Fourth Working Conference on Current Measurement*, G. APPELL and T. B. CURTIN, editors, pp. 258–266.

CANDELA J. M., R. C. BEARDSLEY and R. LIMEBURNER (1992) Separation of tidal and subtidal currents in ship-mounted acoustic Doppler current profiler (ADCP) observations. *Journal of Geophysical Research*, **97**, 769–788.

CHABERT D'HIERES G., H. DIDELLE and D. OBATON (1991) A laboratory study of surface boundary currents: Application to the Algerian Current. *Journal of Geophysical Research*, **96**, 12 539–12 548.

CHAO S.-Y. (1990) Tidal modulation of estuarine plumes. *Journal of Physical Oceanography*, **20**, 1115–1123.

CHATWIN P. C. and C. M. ALLEN (1985) Mathematical models of dispersion in rivers and estuaries. *Annual Review of Fluid Mechanics*, **17**, 119–149.

CUSHMAN-ROISIN B. (1986) Frontal geostrophic dynamics. *Journal of Physical Oceanography*, **16**, 132–143.

DYER K. R. (1973) *Estuaries: a physical introduction*, John Wiley and Sons, London, 140 pp.

FISCHER H. B. (1976) Mixing and dispersion in estuaries. *Annual Review of Fluid Mechanics*, **8**, 107–133.

FISCHER H. B., E. J. LIST, R. C. Y. KOH, J. IMBERGER and N. H. BROOKS (1979) *Mixing in inland and coastal waters*, Academic Press, New York, 483 pp.

FLIERL G. R. (1984) Rossby wave radiation from a strongly nonlinear warm eddy. *Journal of Physical Oceanography*, **14**, 47–58.

FOFONOFF N. P. and H. L. BRYDEN (1985) Density of seawater. *Journal of Marine Research*, **41**, 69–82.

FOREMAN M. G. G. and H. J. FREELAND (1991) A comparison of techniques for tide removal from ship-mounted acoustic Doppler measurements along the southwest coast of Vancouver Island. *Journal of Geophysical Research*, **96**, 17,007–17,021.

FUGLISTER F. C. (1955) Alternative analyses of current surveys. *Deep-Sea Research*, **2**, 213–229.

GALPERIN B. and G. L. MELLOR (1990) A time dependent, three-dimensional model of the Delaware Bay and River system. Part II: Three-dimensional flow field and residual circulation. *Estuarine and Coastal Shelf Science*, **31**, 255–281.

GARVINE R. W. (1991) Subtidal frequency estuary-shelf interaction: Observations near Delaware Bay. *Journal of Geophysical Research*, **96**(C4), 7049–7064.

GARVINE R. W., R. K. MCCARTHY and K.-C. WONG (1992) The axial salinity distribution in the Delaware estuary and its weak response to river discharge. *Estuarine and Coastal Shelf Science*, **35**, 157–165.

GRIFFITHS R. W. and P. F. LINDEN (1981) The stability of buoyancy driven coastal currents. *Dynamics of Atmospheres and Oceans*, **5**, 281–306.

HANSEN D. V. and M. RATTRAY (1965) Gravitational circulation in straits and estuaries. *Journal of Marine Research*, **23**, 104–122.

HOGG N. G. (1973) On the stratified Taylor Column. *Journal of Fluid Mechanics*, **58**, 517–537.

JOHANNESSEN J. A., E. SVENDSEN, S. SANDVEN, O. M. JOHANNESSEN and K. LYGRE (1989) Three dimensional structure of meso-scale eddies in the Norwegian Coastal Current. *Journal of Physical Oceanography*, **19**, 3–19.

JOYCE T. M. (1989) On *in situ* "calibration" of shipboard ADCP's. *Journal of Atmospheric and Oceanic Technology*, **6**, 169–172.

MASSE A. K. (1990) Withdrawal of shelf water into an estuary: A barotropic model. *Journal of Geophysical Research*, **95**, 16 085–16 096.

MELLOR G. L. and T. YAMADA (1982) Development of a turbulence closure model for geophysical fluid problems. *Review of Geophysical and Space Physics*, **20**, 851–875.

MÜNCHOW A. (1992) The formation of a buoyancy driven coastal current, Ph.D. Dissertation, University of Delaware, Newark, DE, 205 pp.

MÜNCHOW A. and R. W. GARVINE (1993a) Buoyancy and wind forcing of a coastal current. *Journal of Marine Research*, **51**, 293–322.

MÜNCHOW A. and R. W. GARVINE (1993b) Dynamical properties of a buoyancy driven coastal current. *Journal of Geophysical Research*, **98**, 20,063–20,077.

MÜNCHOW A., A. K. MASSE and R. W. GARVINE (1992a) Astronomical and nonlinear tidal currents in a coupled estuary shelf system. *Continental Shelf Research*, **12**(4), 471–498.

MÜNCHOW A., R. W. GARVINE and T. F. PFEIFFER (1992b) Subtidal currents from a shipboard acoustic Doppler current profiler in tidally dominated waters. *Continental Shelf Research*, **12**(4), 499–515.

OFFICER C. B. (1976) *Physical oceanography of estuaries (and associated coastal waters)*, John Wiley and Sons, New York, 465 pp.

PAPE E. H., III and R. W. GARVINE (1982) The subtidal circulation in Delaware Bay and adjacent shelf waters. *Journal of Geophysical Research*, **87**, 7955–7970.

PRITCHARD D. W. (1956) The dynamic structure of a coastal plain estuary. *Journal of Marine Research*, **15**, 33–42.

REGIER L. (1982) Mesoscale current fields observed with a shipboard profiling acoustic current meter. *Journal of Physical Oceanography*, **12**, 880–886.

ROYER T. C. (1983) Observations of the Alaskan Coastal Current. In: *Coastal oceanography*, H. GADE, A. EDWARDS, H. SVENDSEN, editors, Plenum Publishing Corporation, New York, 582 pp.

DE RUIJTER W. P. M., A. VAN DER GIESSEN and F. C. GROENENDIJK (1991) Current and density structure in the Netherlands coastal zone. Proceedings, 5th International Conf. on Physics of Estuaries and Coastal Seas, Gregynog, Germany. In: *Coastal and estuarine studies*, **40**, D. PRANDLE, editor, American Geophysical Union, Washington, D.C., pp. 529–550.

SANDWELL D. T. (1987) Biharmonic spline interpolation of GEOS-3 and SEASAT altimeter data. *Geophysical Research Letters*, **14**, 139–142.

SHAFFER G. and L. Djurfeldt (1983) On the low frequency fluctuations in the eastern Skagerrak and Gullmarey. *Journal of Physical Oceanography*, **13**, 1321–1340.

SHARP J. H., L. A. CIFUENTES, R. B. COFFIN, J. R. PENNOCK and K.-C. WONG (1986) The influence of river variability on the circulation, chemistry, and microbiology of the Delaware estuary. *Estuaries*, **9**(4A), 261–269.

SIMPSON J. H., E. G. MITCHELSON-JACOB and A. E. HILL (1990) Flow structure in a channel from an acoustic Doppler current profiler. *Continental Shelf Research*, **10**, 589–603.

SMITH R. (1980) Buoyancy effects upon longitudinal dispersion in wide, well-mixed estuaries. *Philosophical Transactions of the Royal Society London A*, **296**, 467–495.

SOKAL R. R. and F. J. ROHLF (1981) *Biometry*, Freeman, New York, 859 pp.

WONG K.-C. and R. W. GARVINE (1984) Observations of wind-induced, subtidal variability in the Delaware Estuary. *Journal of Geophysical Research*, **89**, 10 589–10 598.

APPENDIX: ADCP PROCESSING AND ANALYSIS

For almost a decade now oceanographers have been using shipboard ADCPs (REGIER, 1982), but only very recently did they survey the coastal ocean with this instrument (SIMPSON *et al.*, 1990). Tidal currents that vary spatially and temporally on the scale of the observations constitute the major problem of coastal ADCP applications. Subtidal currents, too, vary spatially. As a result, the measured flow field is often useless unless one properly separates tidal and subtidal variability with a careful analysis. This appendix outlines a tide removal technique, describes the data set, estimates decorrelation scales, and closes with a discussion of the tidal and subtidal flow that we explain as well as the residual that we do not explain.

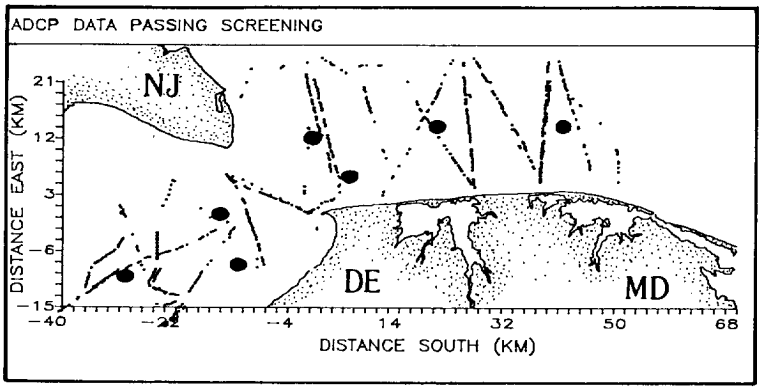

Fig. 15. The locations of the ADCP data and those of the 7 knots of the biharmonic splines (see text).

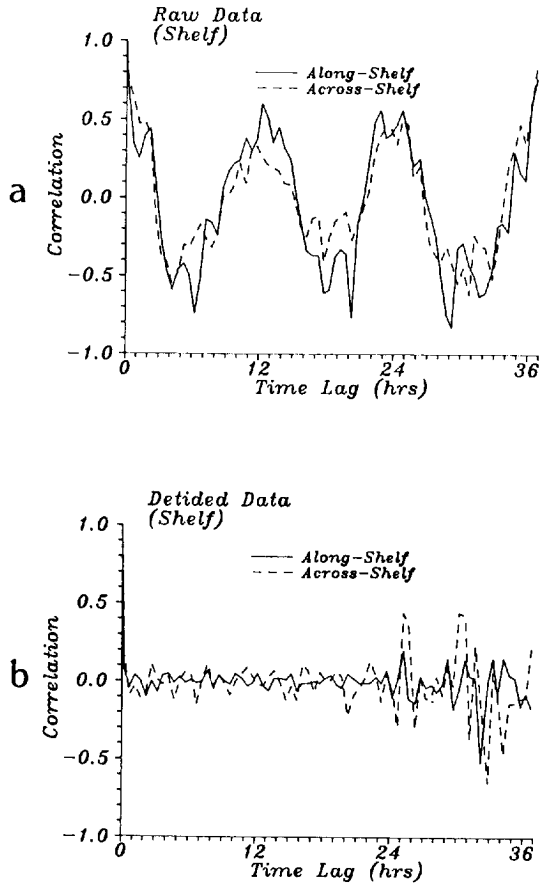

Fig. 16. The normalized cross-correlation of the raw velocity estimates along the ship track (top panel) and that for the detided velocity estimates (lower panel).

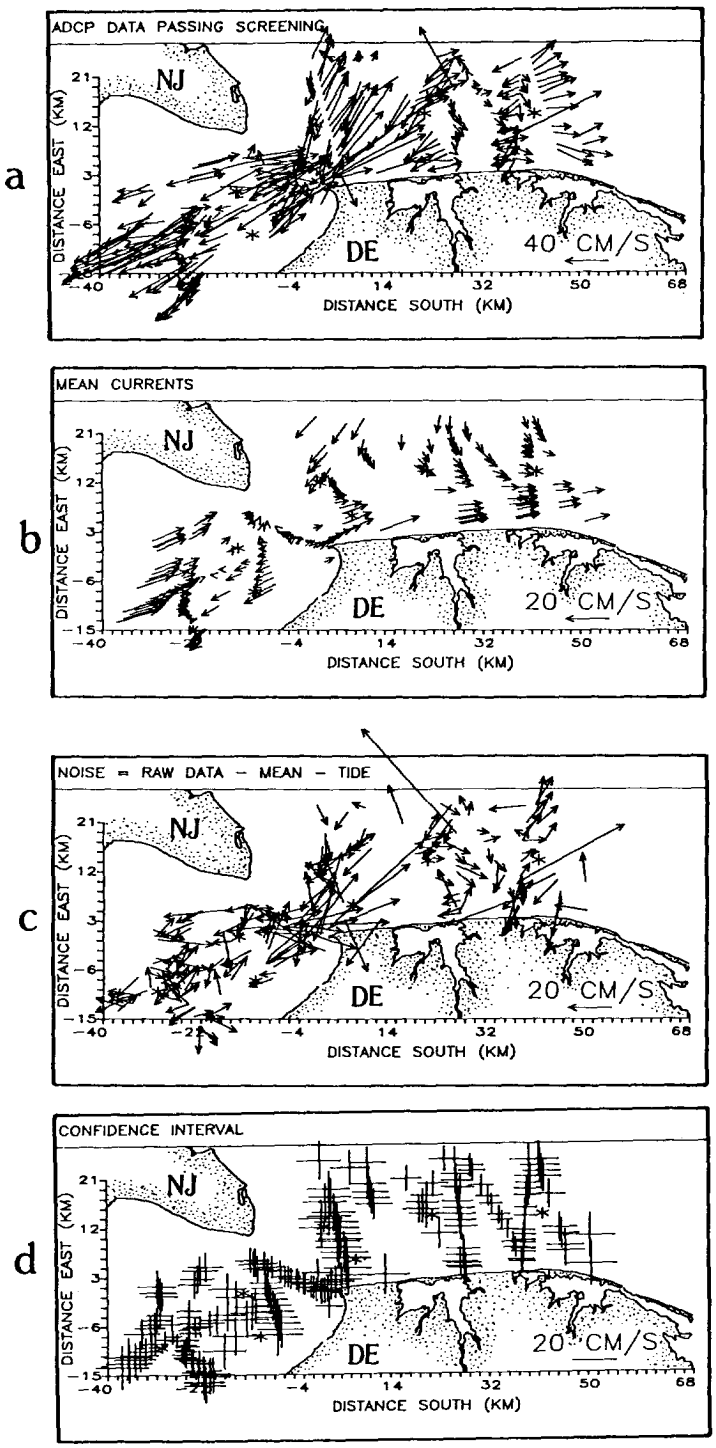
a
ADCP DATA PASSING SCREENING
NJ
DE
40 CM/S
DISTANCE EAST (KM)
DISTANCE SOUTH (KM)
b
MEAN CURRENTS
NJ
DE
20 CM/S
DISTANCE EAST (KM)
DISTANCE SOUTH (KM)
c
NOISE = RAW DATA − MEAN − TIDE
NJ
DE
20 CM/S
DISTANCE EAST (KM)
DISTANCE SOUTH (KM)
d
CONFIDENCE INTERVAL
NJ
DE
20 CM/S
DISTANCE EAST (KM)
DISTANCE SOUTH (KM)

CANDELA *et al.* (1990), FOREMAN and FREELAND (1991) and MÜNCHOW *et al.* (1992b) all tested different methods to remove tidal currents from an ADCP record. Instead of discussing all the details of these methods, we will merely outline the method that we adopted. We prescribe a model that consists of an M_2 tidal constituent with frequency ω, a time independent subtidal current ψ_o and a random noise ε, i.e.

$$\psi(x, y, t) = \psi_o(x, y) + \varepsilon(x, y, t) + [(A(x, y) \cos(\omega t) + B(x, y) \sin(\omega t)] \quad \text{(A1)}$$

where ψ is a current component, $(x, y) = \mathbf{x}$ are horizontal coordinates, t is time, and A, B, and ψ_o are prescribed linear combinations of spatial base functions with unknown coefficients. We choose our base functions to represent biharmonic splines (SANDWELL, 1987).

The model is subjected to a least squares misfit criterion that determines the unknown coefficients at N knot locations (SANDWELL, 1987; CANDELA *et al.*, 1990). Biharmonic splines minimize the curvature (second derivative) of the velocity field (BIGGS, 1974) and therefore smooth behavior of estimated currents between knot locations is guaranteed and is thus not a result.

During our study we collected more than 2800 ADCP profiles at the rate of one profile per minute. We first screened all data and discarded those that either failed to pass the four screening criteria of Table 3 or failed to track the bottom. From the remaining 813 profiles we then computed velocity correlations in order to estimate decorrelation scales and the degrees of freedom of the data set. The locations of the ADCP data and those of the $N = 7$ knots of the biharmonic splines are shown in Fig. 15.

Our model [equation (A1)] assumes that the flow field consists of three independent parts. These are the subtidal current, a tidal current, and random noise. The latter occurs at all time and space scales, i.e. we expect the noise to be broad banded in both frequency and wavenumber space. In order to test this expectation we collect velocity pairs in bins of constant time lag along the ship track, compute the cross-correlation of all velocity pairs in each bin, normalize by the cross-correlation at zero lag, and show the correlations as a function of lag time in Fig. 16. The periodic correlations of the raw data [Fig. 16(a)] emphasize the dominance of the tidal currents. Broad banded noise is manifested by the constant amplitude of the tidal sidelobes (BENDAT and PIERSOL, 1980, p. 57). The noise and the correlations are similar for both velocity components. After subtracting the modeled tidal currents from the raw data, and repeating the lagged correlation analysis on the detided data, we arrive at Fig. 16(b). We draw two conclusions from that figure. First, the biharmonic splines remove the tidal currents very effectively from the raw ADCP data, and second, the decorrelation scales are very small indeed. We note that the detided currents include the subtidal part of the circulation which we cannot distinguish from the noise in the lagged correlations. A spatially uniform mean, however, does not contribute to the correlations. The small decorrelation scale, less than 5 min, allows us to interpret many of the 1 min ADCP samples as uncorrelated and thus statistically independent.

In order to subsequently analyze statistically independent samples only, we further reduce the data set by requiring all our screening criteria to be valid for three successive ADCP samples. We then average the three 1 min samples that pass the test. We finally regard each of the remaining 272 ADCP profiles as uncorrelated. A 3 min average along the ship track corresponds to a spatial average of about 1 km if the ship moves with a speed of 12 knots. This, however, is a lower bound of spatial separation since we screen the data rigorously. The final ADCP record is distributed irregularly in both time and space. Mean sample separations are about 7 min (or 2 km), excluding gaps longer than 1 h.

The least squares fit of the 272 data to the model can be written compactly as

$$K\mathbf{c} = \mathbf{d} \quad \text{(A2)}$$

where K is a real and symmetric $3N \times 3N$ matrix that depends on the tidal frequency and the location of the data and the N knots. The vector $\mathbf{c}$ contains the $3N$ unknown coefficients while $\mathbf{d}$ depends upon the velocity measurements, their locations, and the location of the knots. Solving equation (A2) requires the inversion of K which might, at times, cause problems if the matrix is ill-conditioned or singular. CANDELA *et al.* (1992) proposed to use the method of singular value decomposition, but that is not necessary here. The condition number $R = (\sigma_{max}/\sigma_{min})^{1/2}$ of the matrix equals 770 in our case. $\sigma_{max}/\sigma_{min}$ is the ratio of the largest to the smallest

Fig. 17. (a) ADCP velocity vectors prior to the analysis described in equation (A1), (b) the mean current estimates, (c) the noise as described in equation (A1), (d) the confidence intervals associated with the velocity estimates.

eigenvalue of K and measures how singular that matrix is. The inverse of K constitutes a covariance matrix that is often used to estimate standard errors and confidence limits in multiple regression (FOFONOFF and BRYDEN, 1975; SOKOL and ROHLF, 1980).

Figure 17 shows the 272 ADCP velocity vectors prior to the analysis, the subtidal current ψ_o, the unexplained noise ε, and the 95% confidence limits for the estimates ψ_o. We here interpret the subtidal flow ψ_o as a spatially smoothed version of the true subtidal current. The noise ε is often as large as ψ_o, but it varies randomly in space while ψ_o is almost uniform on the shelf. As the noise variance constitutes only 13% of the total current variance, we conclude that tidal and subtidal currents explain the observed current field well. The confidence limits, however, are rather large and our subtidal results are only marginally significant at the 95% level of confidence. We would like to stress, however, that the subtidal current estimates are consistent with the local hydrography of the shelf, and we thus believe that they describe the dominant subtidal flow reliably there.